Archival Report

Biological Psychiatry: GOS

Differential Impact of Anxious Misery Psychopathology on Multiple Representations of the Functional Connectome

Darsol Seok, Joanne Beer, Marc Jaskir, Nathan Smyk, Adna Jaganjac, Walid Makhoul, Philip Cook, Mark Elliott, Russell Shinohara, and Yvette I. Sheline

ABSTRACT

BACKGROUND: One aim of characterizing dimensional psychopathology is associating different domains of affective dysfunction with brain circuitry. The functional connectome, as measured by functional magnetic resonance imaging, can be modeled and associated with psychopathology through multiple methods; some methods assess univariate relationships while others summarize broad patterns of activity. It remains unclear whether different dimensions of psychopathology require different representations of the connectome to generate reproducible associations.

METHODS: Patients experiencing anxious misery symptomology (depression, anxiety, and trauma; n = 192) received resting-state functional magnetic resonance imaging scans. Three modeling approaches (seed-based correlation analysis, edgewise regression, and brain basis set modeling), each relying on increasingly broader representations of the functional connectome, were used to associate connectivity patterns with six data-driven dimensions of psychopathology: anxiety sensitivity, anxious arousal, rumination, anhedonia, insomnia, and negative affect. To protect against overfitting, 50 participants were held out in a testing dataset, leaving 142 participants as training data.

RESULTS: Different modeling approaches varied in the extent to which they could model different symptom dimensions: seed-based correlation analysis failed to reproducibly model any symptoms, subsets of the connectome (edgewise regression) were sufficient to model insomnia and anxious arousal, and broad representations of the entire connectome (brain basis set modeling) were necessary to model negative affect and ruminative thought.

CONCLUSIONS: These results indicate that different methods of representing the functional connectome differ in the degree that they can model different symptom dimensions, highlighting the potential sufficiency of subsets of connections for some dimensions and the necessity of connectome-wide approaches in others.

https://doi.org/10.1016/j.bpsgos.2021.11.004

The DSM conceptualizes mental illnesses as discrete disorder classes. Notable issues with the DSM, such as heterogeneity within disorders and a lack of understanding of underlying mechanisms, have motivated the development of alternative frameworks such as the Research Domain Criteria (RDoC) (1). Whereas the DSM groups symptoms together based on common co-occurrence, RDoC delineates these symptoms onto distinct dimensions of behavioral and cognitive (dys) function, with the goal of mapping these dimensions onto biological mechanisms. This study applies this dimensional approach to a class of disorders termed disorders of anxious misery (AM) (2,3), which includes DSM diagnoses of generalized anxiety disorder, major depressive disorder, persistent depressive disorder, and posttraumatic stress disorder. Combined, these disorders affect more than 800 million people worldwide and constitute the leading cause of disability (4). Patients with these disorders exhibit dysfunction along various dimensions of neurocognitive functioning (constructs in the RDoC), such as anxiety, frustrative nonreward, and sleep-wakefulness.

A key element for investigating these dimensions is the identification of their underlying neural circuits. Resting-state networks (5,6) can be probed using noninvasive brain imaging to visualize the functional coactivation of specific brain regions, together forming the functional connectome (7). A key challenge in associating psychopathology with the functional connectome is the sheer size of connectomic data: a typical imaging sequence may measure signal from approximately 200,000 voxels, resulting in approximately 10^9 potential components of the connectome (8). Given the potentially massive size of these data, many modeling approaches only use a subset of the total information available within the connectome. At one extreme are univariate seed-based correlation analysis (SCA) approaches, which examine associations

SEE COMMENTARY ON PAGE 316

ISSN: 2667-1743

between behavioral variables and connectivity between just two regions, the selection of which is often determined a priori. In contrast, data-driven models such as edgewise support vector regression (9) typically rely on a small subset of functional connections within the connectome to generate multivariate symptom-brain associations. Finally, recent methods such as brain basis set modeling (BBS) (10) capitalize on connectivity patterns that can span the entire brain, using dimensionality reduction approaches such as principal component analysis (PCA) to efficiently summarize large-scale patterns. It remains an open question whether different modeling approaches are better suited for different dimensions of AM symptomology; dysfunction in a single circuit may be sufficient to model some dimensions, while broader, global patterns of connectivity may be necessary to model other dimensions.

An important consideration in assessing the generalizability of symptom-brain associations is the ability to replicate performance in a held-out testing dataset (11). Systematic examinations of brain-behavior associations have revealed that samples far larger than those typically used in neuroimaging studies of psychopathology may be required to generate stable associations (12). Furthermore, notable examples of failed replications (13,14) have revealed the perils of fitting multivariate models, particularly when models rely on a small subset of functional connections selected through data-driven methods. Many of these failures in replication stemmed from findings that incorrectly applied cross-validation, which requires complete encapsulation of information between folds to generate a reasonable estimate of out-of-sample performance (15). Direct validation of model performance in a held-out sample is therefore an important step to assessing the potential generalizability of any symptom-brain association.

To this end, this work examined transdiagnostic associations between six data-driven dimensions of AM symptomology (anxiety sensitivity, anxious arousal, ruminative thought, anhedonia, insomnia, and negative affect) and functional connectivity using three different modeling approaches. The data were randomly divided into a training set and a held-out testing set to validate model performance.

METHODS AND MATERIALS

Sample Characteristics

For a complete description of sample characteristics, screening procedures, and participant assessment, readers are directed to the reference publication for this dataset (16).

Participants experiencing symptoms of AM (n = 194) were recruited through the community. Healthy comparators (HCs) (n = 48) were also recruited; only one modeling approach (BBS) used data from HC participants. Demographic information is summarized in Table 1, with additional demographic information in Table S1. Two AM participants were removed from analyses due to excessive in-scanner motion, so we present demographics for 192 AM and 48 HC participants.

To ensure a transdiagnostic dataset within the AM category, participants were deemed eligible if their neuroticism score on the Neuroticism-Extraversion-Openness Five-Factor Inventory was greater than one standard deviation above the population mean (≥26.2 for males, ≥30.1 for females) (17). Neuroticism was selected as an eligibility criterion because it captures general elements of psychopathology that are shared by participants diagnosed with depression, anxiety, and trauma-related disorders (18,19).

We did not require participants to cease taking any psychotropic medications. The majority of our study participants (73.4%) were unmedicated. All participants provided informed consent, and all study procedures were conducted under the approval of the University of Pennsylvania Institutional Review Board.

Table 1. Participant Characteristics

Characteristics	Total, N = 240	Control, n = 48	Anxious Misery, n = 192
Sex			
Female	168 (70%)	34	134
Male	72 (30%)	14	58
Age, Years[a]			
18–23	68 (28.3%)	11	57
24–29	91 (37.9%)	23	68
30–35	42 (17.5%)	9	33
36–41	30 (12.5%)	4	26
42–47	3 (1.3%)	1	2
48–53	2 (0.8%)	0	2
54–59	4 (1.7%)	0	4
Race			
Asian	25 (10.4%)	6	19
Black	45 (18.8%)	9	36
Multiracial	13 (5.4%)	2	11
Other	5 (2.1%)	2	3
Undisclosed	8 (3.3%)	0	8
White	144 (60.0%)	29	115
Ethnicity			
Hispanic	17 (7.1%)	3	14
Not Hispanic	219 (91.2%)	45	174
Undisclosed	4 (1.7%)	0	4
Medication Status			
Medicated	–	–	51 (26.5%)
Unmedicated	–	–	141 (73.4%)
Primary DSM-5 Diagnosis			
Major depressive disorder	–	–	91 (47.4%)
Generalized anxiety disorder	–	–	42 (21.9%)
Posttraumatic stress disorder	–	–	39 (20.3%)
Persistent depressive disorder	–	–	13 (6.77%)
Social anxiety disorder	–	–	6 (3.12%)
Cyclothymic disorder	–	–	1 (0.52%)

Values are presented as n or n (%). Additional demographic information can be found in Table S1. Note that control participants were only used in the brain basis set modeling approach.

[a]Median = 26 years.

Participant Assessment

To assess participants' symptom profiles, seven clinician-administered and self-report scales measuring a broad range of depressive and anxious symptomology were administered to AM participants [see full list of assessments in Supplemental Methods and Materials and (16)].

Hierarchical Clustering of Symptoms

To derive data-driven symptom communities from our assessment data, we applied a hierarchical clustering algorithm (20) on the Pearson correlation matrix of the 113 constituent items of our seven instruments, using only data from the AM group. After selecting an appropriate resolution (see Supplemental Methods and Materials for details), we derived symptom dimension scores for each participant by computing the mean across items belonging to each symptom community after *z*-scoring.

Imaging Acquisition

Participants received T1-weighted imaging and four resting-state functional magnetic resonance imaging scans (total acquisition time = 23:01) after their symptom assessments. A summary of imaging parameters and image acquisition protocols are provided in Supplemental Methods and Materials, with full details provided elsewhere (16).

Image Preprocessing

Preprocessing details are provided in Supplemental Methods and Materials and the reference publication for this dataset (16). Two participants, both of whom were AM participants (0.83% of all participants), were removed from resting-state analyses due to excessive in-scanner movement (root-mean-squared movement $>$ median (root-mean-squared movement) $+ 3 \times$ interquartile range).

Overview of Modeling Approaches

We tested the ability of three different modeling approaches, each relying on increasingly dense representations of functional connectomics, to generate robust, generalizable associations between imaging data and symptom dimensions. An overview of each of these modeling approaches is provided (Figure 1), with complete details provided in Supplemental Methods and Materials. Implementations for modeling approaches are available at https://github.com/dseok/anxious_misery_connectomes.

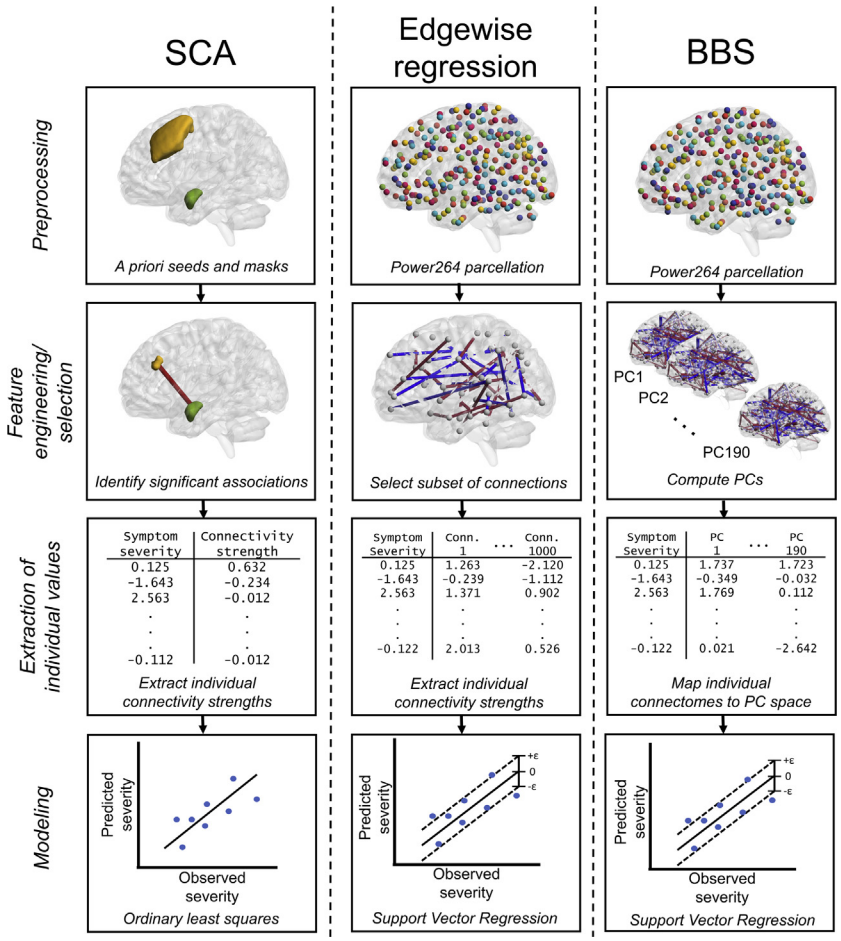

Figure 1. Overview of modeling approaches. All three modeling approaches (seed-based correlation analysis [SCA], edgewise regression, and brain basis set modeling [BBS]) undergo four common steps: 1) preprocessing, wherein the brain is parcellated or masked; 2) feature engineering and selection, wherein specific features are identified or generated; 3) extraction of individual values; and 4) modeling, wherein features are associated with symptom severity. PC, principal component.

Table 2. Seed-Based Correlation Analysis Results

Symptom	References	Seed	Mask	x	y	z	Sign	Voxels, *n*	*r*, Training	*r*, Testing
Anxiety Sensitivity	(28–32)	L amygdala	Whole brain	–	–	–		–	–	–
			L dlPFC	−39	33	31	+	74	0.355	0.337[a]
			R dlPFC	42	33	40	+	8	0.335	0.069
		R amygdala	Whole brain	–	–	–		–	–	–
			L dlPFC	−41	29	35	+	31	0.359	0.241
			R dlPFC	–	–	–		–	–	–
Anxious Arousal	(28–32)	L amygdala	Whole brain	−50	−24	48	−	7	0.376	0.007
			L dlPFC	–	–	–		–	–	–
			R dlPFC	–	–	–		–	–	–
		R amygdala	Whole brain	–	–	–		–	–	–
			L dlPFC	–	–	–		–	–	–
			R dlPFC	30	24	40	−	18	0.326	0.016[a]
Ruminative Thought	(33–36)	PCC	Whole brain	–	–	–		–	–	–
			Precuneus	10	−72	50	+	27	0.345	0.135[a]
			mPFC	–	–	–		–	–	–
Anhedonia	(23–27)	L iVS	Whole brain	–	–	–		–	–	–
			L OFC	–	–	–		–	–	–
			R OFC	–	–	–		–	–	–
		R iVS	Whole brain	–	–	–		–	–	–
			L OFC	−16	38	−16	−	19	0.345	0.276[a]
			R OFC	–	–	–		–	–	–
Negative Affect	(37–44)	sgACC	Whole brain	–	–	–		–	–	–
			Precuneus	–	–	–		–	–	–
			mPFC	–	–	–		–	–	–
			PCC	–	–	–		–	–	–
Insomnia	(45–49)	L insula	Whole brain	–	–	–		–	–	–
			Precuneus	–	–	–		–	–	–
			mPFC	11	69	5	+	111	0.384	0.272[a]
		R insula	Whole brain	–	–	–		–	–	–
			Precuneus	–	–	–		–	–	–
			mPFC	11	70	3	+	37	0.353	0.245

Unique seeds and masks for each symptom cluster (in addition to a whole-brain analysis) were assigned based on findings from extant literature ("Reference"). Whole-brain analyses indicate exploratory analyses wherein significant clusters were permitted anywhere in gray matter. Significant clusters were identified using a nonparametric permutation testing technique incorporating threshold-free cluster enhancement (implemented in FSL's Randomise; FWER < 0.05). Coordinates for cluster center of mass are in MNI space. In the Sign column, the sign indicates the direction of association: "+" indicates that hyperconnectivity was associated with worse symptoms, while "−" indicates that hypoconnectivity was associated with worse symptoms. *r* (training) and *r* (testing) indicate Pearson correlations between observed and predicted symptom scores using a linear model using connectivity *z* scores.

dlPFC, dorsolateral prefrontal cortex; FWER, familywise error rate; iVS, inferior ventral striatum; L, left; MNI, Montreal Neurological Institute; mPFC, medial prefrontal cortex; OFC, orbitofrontal cortex; PCC, posterior cingulate cortex; R, right; sgACC, subgenual anterior cingulate cortex.

[a]Highest performing connections in the testing set for each symptom.

Modeling Approach 1: SCA

SCA associates behavioral variables (in our case, symptom dimension scores) with connectivity between a seed region and another region. Each symptom dimension was assigned specific seeds and masks based on extant literature (Table 2). Exploratory whole-brain analyses (wherein significant clusters outside of a priori masks are permitted) were also conducted.

Clusters that exhibited significant associations based on permutation testing ($p < .05$) are reported. Given that SCA was merely used to identify clusters for further validation in our testing set, this *p*-value threshold was not adjusted for multiple tests; Bonferroni correction of this *p*-value threshold resulted in no significant clusters being identified in the training set. After clusters were identified, linear models predicting symptom severity using connectivity were constructed using mean connectivity between the seed region and the identified cluster; significance of testing performances was corrected (Holm-Bonferroni) separately for each symptom cluster.

Multivariate Methods

The next two modeling approaches used the Power264 atlas, a well-validated parcellation that identifies 264 functional nodes of the brain (21). In addition to these 264 nodes, we supplemented 14 additional nodes relevant to AM disorders, adopted from the additional nodes used in (22) (full table of additional seeds in Table S3).

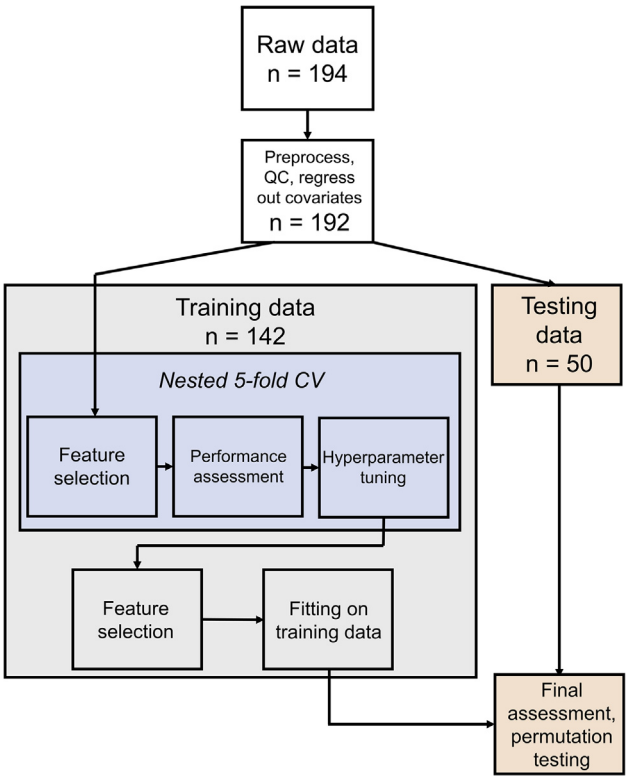

Figure 2. Flowchart of model assessment framework. Two participants were removed for excessive in-scanner motion during quality control (QC) procedures. After data are split into training and testing partitions, hyperparameter tuning in training data is accomplished using nested fivefold cross-validation (CV). The best-performing hyperparameters are used in a final model that is fit on the full training dataset. Finally, model performance is assessed using the testing data, and significance is determined using permutation testing. This process was repeated for each symptom dimension, each time using the same training/testing partition.

For both of the following methods, we extracted the mean time series of each node using spherical regions of interest (5-mm radius) and then computed the Pearson correlation between each time series to generate a 278 × 278 functional connectivity matrix for each scan (38,503 unique connections). Because participants completed four scans, the four resulting matrices were averaged to generate one matrix per participant.

Modeling Approach 2: Edgewise Regression

In this modeling approach, a subset of individual connection strengths (edges) was first selected using a cross-validated feature selection procedure and then associated with symptom severity using support vector regression (linear kernel). Our feature selection procedure indicated that edgewise regression models performed best with a small subset of connectivity features (approximately 5% of the full matrix).

Modeling Approach 3: BBS

BBS (10) uses PCA to generate a low-dimensional representation of interindividual differences in global connectivity patterns. After PCA, support vector regression (linear kernel) was used to associate each symptom dimension with connectivity component scores. To capture directions of connectivity variance that extend into healthy ranges, BBS uses data from HC participants; this was the only modeling approach that used our sample of HCs. PCA was only ever conducted within the training set to prevent data leakage from testing participant data.

Modeling Assessment Framework

All models underwent the following assessment framework (Figure 2) designed to test the performance of models on new, unseen data. First, age, sex, and motion (root-mean-squared) were regressed from connectivity matrices, and age and sex were regressed from symptom scales (see Figures S4 and S5 for correlations with motion and temporal signal-to-noise ratio). No significant associations between symptom scales and motion or temporal signal-to-noise ratio were detected. Second, while matching for age, sex, and symptom severity (see Supplemental Methods and Materials for details), a random subset of 50 AM participants were segregated to a testing set, leaving 142 AM participants for our training set. Next, within the training set, fivefold cross-validation was used to perform feature selection and hyperparameter tuning for the multivariate methods. Connections were selected for each symptom dimension by computing the Spearman correlation between each connection and the symptom dimension in question and then selecting the p connections with the highest absolute correlations, where p is a hyperparameter tuned through nested cross-validation.

Finally, model performance was assessed in the held-out testing set by computing the Pearson correlation between the predicted and actual symptom scores, using a model fit on the entire training set. Significance was determined using a permutation testing procedure wherein null distributions of correlations were generated by shuffling the rows of imaging data relative to symptom data in the training set, performing the entire model-fitting process using this permuted dataset and using this model to compute the correlation between predicted and actual symptom scores in the testing dataset, repeating this entire process 5000 times for each symptom and modeling approach. Given that each symptom dimension is being modeled using three different approaches, final model performances for each symptom were adjusted for multiple testing using separate Holm-Bonferroni corrections.

RESULTS

Symptom Clustering

Inspection of the symptom hierarchy revealed that items clustered according to clinically relevant dimensions (see Figure S1 for complete hierarchy). Symptoms first separated into two large communities, one with predominantly depressive symptoms and the other with largely anxiety-related symptoms. At finer resolutions, these two larger communities separated into three subcommunities each, resulting in six total communities (Figure 3). Anxiety-related symptoms divided into the following communities: anxiety sensitivity (representative item: “It scares me when my heart beats rapidly.”), anxious arousal (“Hands were shaky”), and ruminative thought (“I can’t stop thinking about some things.”).

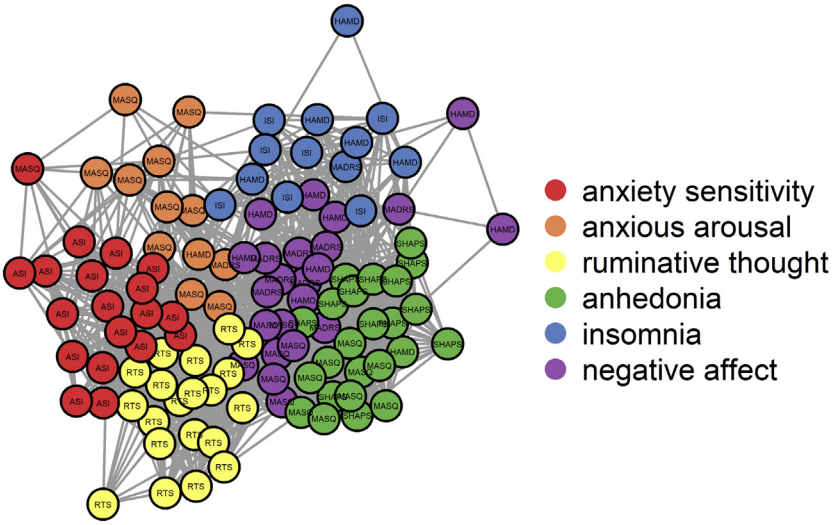

Figure 3. Clustering revealed six communities of symptoms. Each circle represents an item on one of seven patient assessments of psychopathology. Indicated in each circle is the assessment to which the item belongs. Connections and proximity of circles indicate the strength of correlation between items. ASI, Anxiety Sensitivity Index; HAMD, Hamilton Depression Rating Scale; ISI, Insomnia Severity Index; MADRS, Montgomery–Åsberg Depression Rating Scale; MASQ, Anxiety Depression Distress Inventory-27; RTS, Ruminative Thought Style Questionnaire; SHAPS, Snaith-Hamilton Pleasure Scale.

Depression-related symptoms divided into the following communities: anhedonia ("I would not find pleasure in my hobbies and pastimes."), insomnia ("Difficulty falling asleep"), and negative affect ("Pessimistic thoughts"). See Table S4 for a complete list of symptom clusters and their constitutive items. Ultimately, this resolution was chosen for analysis because it 1) allowed for interrogation of symptom dimensions finer than those aligned with traditional diagnostic categories (i.e., anxiety and depressive disorders) and 2) resulted in communities that were broadly aligned with constructs of the RDoC, unlike finer resolutions that split groups of symptoms into clusters too narrow to be meaningfully interpreted. See Figure S3 for correlations between symptom clusters. As expected (2), all symptoms exhibited moderate, positive correlations with each other.

Training and Testing Partitions

Training (n = 142) and testing (n = 50) partitions were well matched for age, sex, and z-scored symptom scores (Figure S2). Two-sample t tests and χ^2 tests did not indicate significant differences between data partitions for all categories.

SCA Results

The complete list of significant clusters identified using SCA is detailed in Table 2. Only one significant cluster was identified using an exploratory whole-brain search, and association with this cluster did not replicate in the testing dataset (anxious arousal, left amygdala ↔ left primary motor cortex, $r_{testing}$ = 0.007, $p_{uncorrected}$ = .962).

With the exception of negative affect, all symptom dimensions identified at least one significantly associated cluster within the training set. However, replication within the testing data was mixed. Only clusters for anxiety sensitivity (left amygdala ↔ left dorsolateral prefrontal cortex, $r_{testing}$ = 0.337, $p_{uncorrected}$ = .017) and anhedonia (right inferior ventral striatum ↔ left orbitofrontal cortex, $r_{testing}$ = 0.276, $p_{uncorrected}$ = .049) generated meaningful correlations in the testing set. Other symptoms, such as anxious arousal (right amygdala ↔ right dorsolateral prefrontal cortex, $r_{testing}$ = 0.016, $p_{uncorrected}$ = .909), completely failed to replicate in the testing set.

Multivariate Models: Hyperparameter Tuning in the Training Dataset

Hyperparameter tuning was accomplished using nested cross-validation within the training dataset (Figure S6). This procedure indicated that edgewise regression models generally favored smaller numbers of connections (approximately 500). In contrast, BBS models favored a high number of connections (approximately 38,000). Because BBS models generally exhibited increasing performance with more features, the full connectivity matrix was used for all BBS models.

BBS: Distribution of Principal Components. Alignment of BBS connectivity component weights with intrinsic connectivity networks was examined (Figure S7). While the first principal components exhibited greater mean loading on a small subset of networks (10), all components exhibited significant loading on multiple networks, suggesting that the interindividual variability captured by BBS components did not merely recapitulate the structure of intrinsic connectivity networks.

BBS: Inclusion of HCs. BBS is the only modeling approach that used HCs. Examination of testing performance with and without HCs revealed that the inclusion of HCs significantly improved performance for negative affect and rumination and had little effect for other symptom dimensions (Figure S8); as such, HCs were included in all BBS models.

Final Model Performance in the Testing Dataset

Final model performance for all three modeling approaches is detailed in Table 3. SCA models failed to replicate for all symptom dimensions. Insomnia ($r_{testing}$ = 0.344, $p_{corrected}$ =

.018) and anxious arousal ($r_{testing}$ = 0.336, $p_{corrected}$ = .027) were only significantly modeled using edgewise regression models. Negative affect ($r_{testing}$ = 0.323, $p_{corrected}$ = .010) and ruminative thought ($r_{testing}$ = 0.313, $p_{corrected}$ = .045) were only significantly modeled by BBS models. Schematic representations of these symptoms and their best performing modeling approaches are displayed in Figure 4. Scatterplots of predicted and observed severities indicated normal distributions and absence of significant outliers (Figure S9).

While modeling approaches were fit independently, connections weighted heavily in simpler models were also prominent in more complex modeling approaches. For example, a priori connections tested in SCA generally exhibited strong weights in multivariate models: for insomnia, the left insula ↔ medial prefrontal cortex connection was in the top 4.04% of connections in its BBS model; for ruminative thought, the precuneus ↔ posterior cingulate cortex connection was in the top 10.05% of connections in its BBS model (and this connection performed comparatively worse in SCA, with $r_{testing}$ = 0.135). Only anxious arousal did not exhibit strong correspondence between its SCA model (which had poor replication in the testing set: $r_{testing}$ = 0.016) and its multivariate models: edgewise regression did not select the right amygdala ↔ right dorsolateral prefrontal cortex connection, and this connection was only in the top 34.01% of connection weights in BBS. Finally, connection weights from edgewise regression models highly correlated with the subset of overlapping connection weights in the equivalent BBS model (range across six symptoms: r = 0.852–0.949).

Network-level representations reveal common and distinct patterns of connectivity abnormalities associated with each symptom dimension (Figure 5). Of the four symptoms best represented by multivariate models, all exhibited abnormal connectivity patterns in the default mode network (DMN). Anxious arousal was characterized by hyperconnectivity between bilateral regions of the DMN, as well as hyperconnectivity between 1) sensory regions such as the visual and auditory cortices and 2) networks in association cortex, such as the cinguloopercular network (CIN), frontoparietal network (FPN), and DMN. Insomnia was associated with hyperconnectivity between the 1) DMN and 2) visual and auditory cortices, the right salience network, and limbic nodes. Ruminative thought was associated with hyperconnectivity between bilateral regions of the CIN, as well as hyperconnectivity between the CIN and visual cortex and hypoconnectivity between the right CIN and the DMN. Finally, negative affect was associated with decreased segregation (increased connectivity) between the left FPN and the DMN, as well as between the CIN and DMN. In addition, the left FPN exhibited decreased connectivity with the salience network and the visual cortex.

DISCUSSION

This work examines transdiagnostic associations between functional connectivity and different symptom dimensions, in line with the dimensional perspective espoused by the RDoC framework (1). Our multimodeling approach suggests that different dimensions of psychopathology required different representations of the functional connectome. Univariate relationships failed to robustly model any symptom dimensions.

Table 3. Pearson's Correlations Between Actual and Predicted Symptom Constructs in the Held-Out Testing Set Using Three Different Modeling Approaches

Symptom	SCA				Edgewise Regression				BBS			
	$r_{testing}$	$p_{uncorrected}$[a]	p	Connections, n	$r_{testing}$	$p_{uncorrected}$	p	Connections, n	$r_{testing}$	$p_{uncorrected}$	p	Connections, n
Anxiety Sensitivity	0.337[b]	.048	.144	1	0.225	.062	.144	500	0.052	.376	.376	38,503
Anhedonia	0.276[b]	.049	.147	1	0.185	.097	.194	500	0.095	.264	.264	38,503
Insomnia	0.272	.117	.117	1	0.344[b,c]	.006	.018	4600	0.246	.041	.082	38,503
Anxious Arousal	0.016	1.000	1.000	1	0.336[b,c]	.009	.027	1200	0.143	.164	.328	38,503
Negative Affect	–	–	–	–	0.016	.449	.449	140	0.367[b,c]	.005	.010	38,503
Ruminative Thought	0.135	.360	.360	1	0.167	.136	.272	3000	0.310[b,c]	.015	.045	38,503

Displayed are uncorrected and corrected (Holm–Bonferroni) permutation-based p values where rows of imaging data were shuffled relative to symptom data in the training set, and the resulting trained models were used to predict testing set symptom data (repeated 5000 times for each symptom and modeling approach). Also listed are the number of functional connections used for each model.

BBS, brain basis set modeling; SCA, seed-based correlation analysis.

[a]Uncorrected p values for SCA have been corrected (Holm-Bonferroni) for multiple clusters for each symptom (see Methods and Materials for more details).

[b]Best-performing model approaches for each symptom construct. For SCA, the best-performing association for each symptom was selected.

[c]Correlation was significant at $p < .05$.

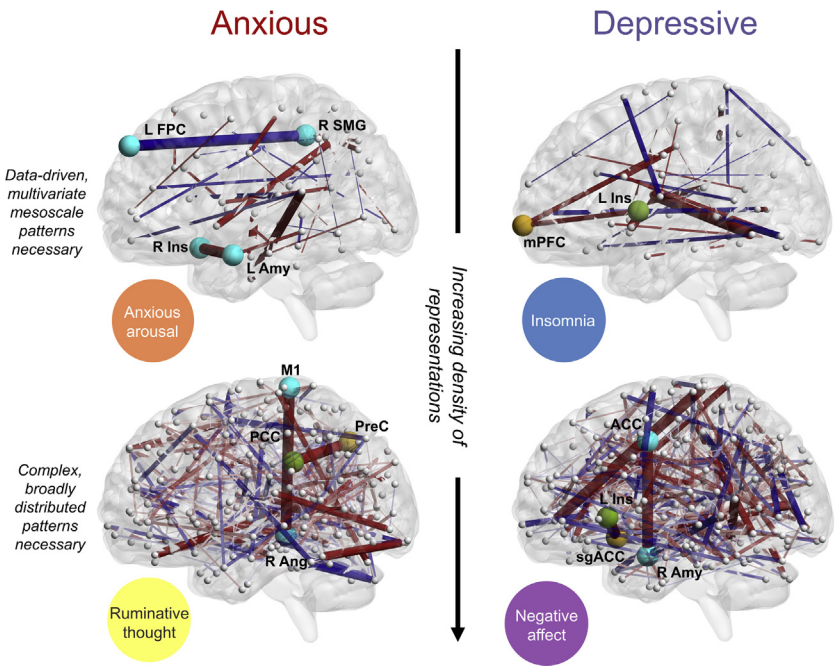

Figure 4. Schematic representations of each symptom and its best-performing modeling approach. Symptoms in the first row were modeled using edgewise regression and in the second row using brain basis set modeling (BBS). A connection's color represents either hyperconnectivity (red) or hypoconnectivity (blue), and a connection's width represents the magnitude of its associated model weight. Green and yellow nodes denote the a priori connections tested in seed-based correlation analysis models; green nodes represent seeds while yellow nodes represent resulting clusters. Other nodes belonging to key connections are labeled and colored cyan for easier identification: anxious arousal was associated with hypoconnectivity between left (L) frontopolar cortex (FPC) and right (R) supramarginal gyrus (SMG) and hyperconnectivity between R insula (Ins) and L amygdala (Amy), ruminative thought was associated with hyperconnectivity between primary motor cortex (M1) and R angular gyrus (Ang), and negative affect was associated with hyperconnectivity between R Amy and anterior cingulate cortex (ACC). For edgewise regression and BBS models, connections in the strongest 1% of model weights are plotted for display purposes (approximately 30 connections for edgewise regression, approximately 300 for BBS models). mPFC, medial prefrontal cortex; PCC, posterior cingulate gyrus; PreC, precuneus; sgACC, subgenual anterior cingulate cortex.

Some dimensions, such as insomnia and anxious arousal, were sufficiently modeled by subsets of the connectome. Other dimensions, such as negative affect and rumination, required information from the entire connectome; for these dimensions, smaller subsets of connectome were not sufficient to generate a replicable association.

Anhedonia and anxiety sensitivity were not reproducibly modeled by any of our modeling approaches, despite a broad body of work implicating specific connections for both anhedonia (23-27) and anxiety sensitivity (28–32). In fact, all associations from single connections failed to replicate in the testing set after correction for multiple comparisons. This finding recapitulates similar studies that have highlighted the challenges of replicating univariate associations in fully held-out samples (12).

In contrast to anhedonia and anxiety sensitivity, anxious arousal and insomnia were sufficiently modeled using edgewise regression, which used a small subset of the connectome (~5%). Similar to anxiety sensitivity, anxious arousal has been associated with abnormal amygdala connectivity (30,50). However, cross-cultural studies have revealed that different ethnoracial groups experience different degrees of anxious arousal (somatization), suggesting that this symptom dimension likely involves cortical integration beyond the amygdala (50,51). Indeed, anxious arousal was associated with hyperconnectivity between sensory regions and regions in the association cortex (including the CIN, FPN, and DMN), which may underlie the somatization of anxious states. Insomnia was associated with hyperconnectivity between the DMN and multiple cortical areas, including the primary sensory cortex, salience network, and limbic nodes. This exaggerated connectivity with the DMN may represent increased vigilance and awareness of emotional and bodily states, resulting in poor sleep initiation and continuity (52).

Finally, two of our constructs, rumination and negative affect, were only robustly modeled by BBS, which used information from the entire connectome and drew from components with broad alignments with multiple intrinsic connectivity networks. Evolutionary theories of ruminative thought support the notion that this symptom dimension likely developed later in evolution because the emergence of complex social environments and the ability to engage in sustained processing are thought to be supported by the expansive primate neocortex (53,54). Similar theories about negative affectivity suggest that stress drives the brain to reorganize to minimize surprise (prediction error) in the environment, a complex process that likely involves cortex-spanning, multinetwork interactions (55). Both ruminative thought and negative affect exhibited abnormalities with the DMN, which has been consistently implicated in AM disorders, particularly in depression (37,56). Hyperactivity of the DMN during emotional perception and judgment (57) and passive viewing and reappraisal of negative pictures (56) as well hyperconnectivity between the DMN and the FPN (38) suggest that DMN abnormalities may underlie an inability to detach from internal emotional states [e.g., rumination and negative affect (56)].

This is not to suggest, however, that the nonoptimal modeling approaches are without merit. While only the highest performing models for each symptom survived testing for multiple comparisons (with the exception of SCA models; see Figure S10 for schematic diagrams of all six symptom dimensions and their best performing models), different models

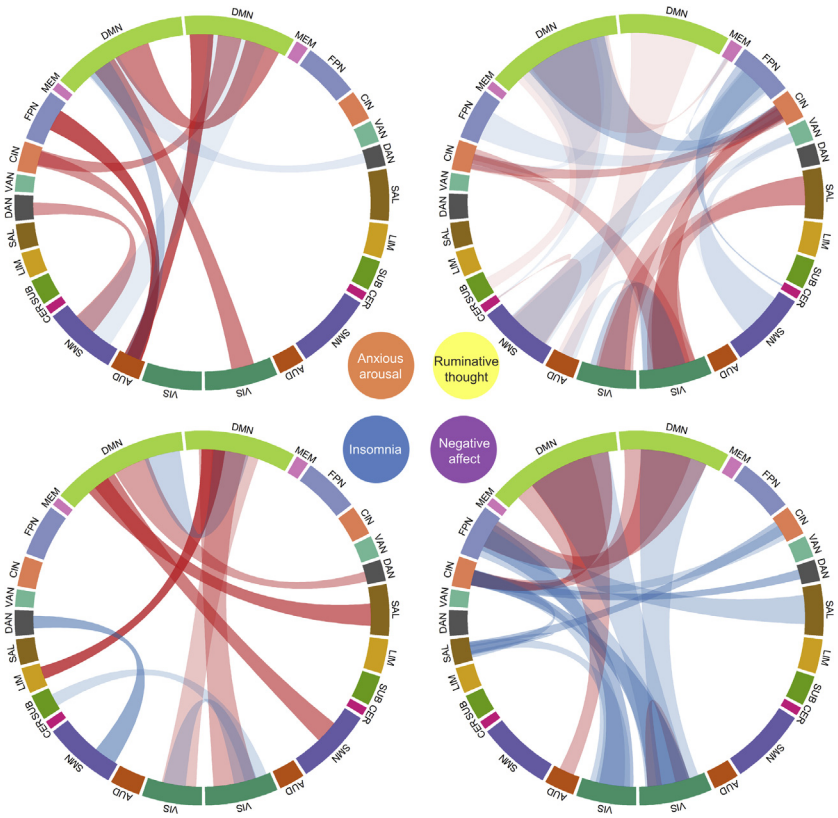

Figure 5. Chord diagrams displaying network-level associations for symptoms best fit by multivariate models. Association strengths were collated by node community, according to the a priori communities delineated in the Power264 atlas. Communities were lateralized and plotted around each chord diagram, with left-lateralized nodes displayed on the left side of the plot and bar width proportional to the number of nodes in the community. Red ribbons indicate hyperconnectivity, while blue ribbons indicate hypoconnectivity in association with symptom scores. Ribbon opacity is proportional to the mean strength of association with the symptom dimension (more opaque = stronger association), and ribbon width is proportional to the number of connections participating in a plotted association (wider ribbon = more connections). Ribbon appearance was determined based on a formula that balanced 1) the mean strength of connections, 2) the variability of these connection strengths, and 3) the number of connections of each community-pair. Full details for how this visualization was generated can be found in Supplemental Methods and Materials (Chord diagram for multivariate models). Note that the left column of diagrams represents edgewise regression models, while the right column represents brain basis set modeling models. AUD, auditory; CER, cerebellar; CIN, cinguloopercular network; DAN, dorsal attention network; DMN, default mode network; FPN, frontoparietal network; LIM, limbic; MEM, memory retrieval; SAL, salience network; SMN, somatomotor network; SUB, subcortical; VAN, ventral attention network; VIS, visual.

of the same symptom exhibited similar weights, suggesting that convergent signals informed these different models. Furthermore, differences in model performance for some symptom dimensions were relatively minor; for example, all modeling approaches for insomnia performed relatively well. While the use of permutation testing, validation in a held-out dataset, and correction for multiple comparisons helps to confirm the validity of each individual model, the comparison of performances between models is by no means conclusive without rigorous statistical tests that would require larger sample sizes. Future analyses in larger datasets using iterative cross-validation methods are necessary to confirm these hypotheses.

Direct validation of our models in a held-out dataset was critical for verifying their performance. Indeed, edgewise regression models exhibited excellent performance in training set cross-validation (typically achieving correlations of 0.6) but did not generate significant associations in testing data for four of six symptom dimensions. Edgewise regression favored smaller subsets of features, typically on the order of 500 features (around approximately 1% of the full connectivity matrix), which is similar to the number of connections used in many other studies examining multivariate associations of psychopathology (22,58–60). Notably, many of these studies did not perform a direct validation of their models on held-out data which, as the results from this study suggest, is a crucial step in assessing the generalizability of multivariate models.

While we strove to implement a rigorous analytic design and findings are reinforced by and expand on prior literature, these results should also be considered in the context of the following limitations. To minimize the number of hypotheses tested for SCA, we limited seeds and masks for SCA to a circumscribed set based on extant literature. It is possible that univariate connections outside of those tested could replicate in a testing set. However, we took care to focus on those connections that were best supported by the literature. Furthermore, exploratory whole-brain analyses only generated one cluster (anxious arousal; left amygdala ↔ left primary motor cortex), which failed to replicate in the testing dataset. In addition, most seed regions used for SCA were defined using anatomical atlases; it has been demonstrated that functional regions may be better captured through different means (61,62), and the use of alternative seeds in future studies may yield stronger results for SCA. Additional limitations include the theory-driven selection of symptom structure resolution; other resolutions in the symptom hierarchy could reveal additional insights. Entirely data-driven multiview analyses that simultaneously model symptom structures and associated connectivity patterns are possible (63). However, recent simulation studies suggest that very high sample sizes (approaching thousands of individuals for an $r = 0.3$) may be necessary to generate reproducible associations using these methods (64). Given our sample size ($n = 192$), we chose instead to fix our symptom structure based on the emergence of psychologically plausible, coherent symptom communities. Finally, the

testing dataset was of moderate size (n = 50); future analyses pooling data from multiple sites will prove invaluable for testing the robustness and generalizability of symptom-brain associations (12).

Despite these limitations, this work represents one of the only studies to examine transdiagnostic AM psychopathology using multiple representations of brain connectivity. Our rigorous performance assessment framework revealed that different dimensions of AM psychopathology required different representations of functional connectivity, highlighting the potential sufficiency of single-circuit, univariate approaches for some dimensions and the necessity of connectome-wide, multivariate approaches in others.

ACKNOWLEDGMENTS AND DISCLOSURES

This work was supported by the National Institute of Mental Health Grant No. U01 MH109991 (to YIS).

We acknowledge Maria Prociuk for her help in preparing the manuscript for publication. We also thank all participants for their participation.

A previous version of this article was published as a preprint on bioRxiv: https://www.biorxiv.org/content/10.1101/2021.03.05.434151v1.

The authors report no biomedical financial interests or potential conflicts of interest.

ARTICLE INFORMATION

From the Center for Neuromodulation in Depression and Stress (DS, MJ, NS, AJ, WM, RS, YIS), Department of Psychiatry; Penn Statistics in Imaging and Visualization Center (JB, RS), Department of Biostatistics, Epidemiology, and Informatics; Department of Radiology (PC, ME, YIS); Center for Biomedical Image Computing and Analytics (RS); and the Department of Psychiatry (YIS), Perelman School of Medicine, University of Pennsylvania, Philadelphia, Pennsylvania.

Address correspondence to Yvette I. Sheline, M.D., M.S., at sheline@pennmedicine.upenn.edu.

Received Aug 26, 2021; revised Nov 3, 2021; accepted Nov 7, 2021.

Supplementary material cited in this article is available online at https://doi.org/10.1016/j.bpsgos.2021.11.004.

REFERENCES

1. Insel T, Cuthbert B, Garvey M, Heinssen R, Pine DS, Quinn K, *et al.* (2010): Research domain criteria (RDoC): Toward a new classification framework for research on mental disorders. Am J Psychiatry 167:748–751.
2. Krueger RF (1999): The structure of common mental disorders. Arch Gen Psychiatry 56:921–926.
3. Watson D (2005): Rethinking the mood and anxiety disorders: A quantitative hierarchical model for DSM-V. J Abnorm Psychol 114:522–536.
4. Murray CJL, Atkinson C, Bhalla K, Birbeck G, Burstein R, Chou D, *et al.* (2013): The state of US health, 1990–2010: Burden of diseases, injuries, and risk factors. JAMA 310:591–608.
5. Biswal B, Yetkin FZ, Haughton VM, Hyde JS (1995): Functional connectivity in the motor cortex of resting human brain using echo-planar MRI. Magn Reson Med 34:537–541.
6. Fox MD, Raichle ME (2007): Spontaneous fluctuations in brain activity observed with functional magnetic resonance imaging. Nat Rev Neurosci 8:700–711.
7. Van Dijk KRA, Hedden T, Venkataraman A, Evans KC, Lazar SW, Buckner RL (2010): Intrinsic functional connectivity as a tool for human connectomics: Theory, properties, and optimization. J Neurophysiol 103:297–321.
8. Glasser MF, Sotiropoulos SN, Wilson JA, Coalson TS, Fischl B, Andersson JL, *et al.* (2013): The minimal preprocessing pipelines for the Human Connectome Project. Neuroimage 80:105–124.
9. Davatzikos C (2019): Machine learning in neuroimaging: Progress and challenges. Neuroimage 197:652–656.
10. Sripada C, Angstadt M, Rutherford S, Kessler D, Kim Y, Yee M, Levina E (2019): Basic units of inter-individual variation in resting state connectomes. Sci Rep 9:1900.
11. Schnack HG, Kahn RS (2016): Detecting neuroimaging biomarkers for psychiatric disorders: Sample size matters. Front Psychiatry 7:50.
12. Marek S, Tervo-Clemmens B, Calabro FJ, Montez DF, Kay BP, Hatoum AS, *et al.* (2022): Reproducible brain-wide association studies require thousands of individuals [published correction appears in Nature 2022; 605(7911):E11]. Nature 603(7902):654–660.
13. Müller VI, Cieslik EC, Serbanescu I, Laird AR, Fox PT, Eickhoff SB (2017): Altered brain activity in unipolar depression revisited: Meta-analyses of neuroimaging studies. JAMA Psychiatry 74:47–55.
14. Dinga R, Schmaal L, Penninx BWJH, van Tol MJ, Veltman DJ, van Velzen L, *et al.* (2019): Evaluating the evidence for biotypes of depression: Methodological replication and extension of Drysdale et al. Neuroimage Clin 22:101796.
15. Poldrack RA, Huckins G, Varoquaux G (2020): Establishment of best practices for evidence for prediction: A review. JAMA Psychiatry 77:534–540.
16. Seok D, Smyk N, Jaskir M, Cook P, Elliott M, Girelli T, *et al.* (2020): Dimensional connectomics of anxious misery, a human connectome study related to human disease: Overview of protocol and data quality. Neuroimage Clin 28:102489.
17. McCrae RR, Costa PT Jr (2007): Brief versions of the NEO-PI-3. J Individ Differ 28:116–128.
18. Andrews G, Stewart G, Morris-Yates A, Holt P, Henderson S (1990): Evidence for a general neurotic syndrome. Br J Psychiatry 157:6–12.
19. Khan AA, Jacobson KC, Gardner CO, Prescott CA, Kendler KS (2005): Personality and comorbidity of common psychiatric disorders. Br J Psychiatry 186:190–196.
20. Jeub LGS, Sporns O, Fortunato S (2018): Multiresolution consensus clustering in networks. Sci Rep 8:3259.
21. Power JD, Cohen AL, Nelson SM, Wig GS, Barnes KA, Church JA, *et al.* (2011): Functional network organization of the human brain. Neuron 72:665–678.
22. Drysdale AT, Grosenick L, Downar J, Dunlop K, Mansouri F, Meng Y, *et al.* (2017): Resting-state connectivity biomarkers define neurophysiological subtypes of depression [published correction appears in Nat Med 2017; 23:264]. Nat Med 23:28–38.
23. Keller J, Young CB, Kelley E, Prater K, Levitin DJ, Menon V (2013): Trait anhedonia is associated with reduced reactivity and connectivity of mesolimbic and paralimbic reward pathways. J Psychiatr Res 47:1319–1328.
24. Satterthwaite TD, Kable JW, Vandekar L, Katchmar N, Bassett DS, Baldassano CF, *et al.* (2015): Common and dissociable dysfunction of the reward system in bipolar and unipolar depression. Neuropsychopharmacology 40:2258–2268.
25. Felger JC, Li Z, Haroon E, Woolwine BJ, Jung MY, Hu X, Miller AH (2016): Inflammation is associated with decreased functional connectivity within corticostriatal reward circuitry in depression. Mol Psychiatry 21:1358–1365.
26. Ferenczi EA, Zalocusky KA, Liston C, Grosenick L, Warden MR, Amatya D, *et al.* (2016): Prefrontal cortical regulation of brainwide circuit dynamics and reward-related behavior. Science 351:aac9698.
27. Rzepa E, McCabe C (2018): Anhedonia and depression severity dissociated by dmPFC resting-state functional connectivity in adolescents. J Psychopharmacol 32:1067–1074.
28. Laeger I, Dobel C, Dannlowski U, Kugel H, Grotegerd D, Kissler J, *et al.* (2012): Amygdala responsiveness to emotional words is modulated by subclinical anxiety and depression [published correction appears in Behav Brain Res 2014; 261:369–370]. Behav Brain Res 233:508–516.
29. Prater KE, Hosanagar A, Klumpp H, Angstadt M, Phan KL (2013): Aberrant amygdala-frontal cortex connectivity during perception of fearful faces and at rest in generalized social anxiety disorder. Depress Anxiety 30:234–241.

30. Liu WJ, Yin DZ, Cheng WH, Fan MX, You MN, Men WW, *et al.* (2015): Abnormal functional connectivity of the amygdala-based network in resting-state FMRI in adolescents with generalized anxiety disorder. Med Sci Monit 21:459–467.
31. Dong M, Xia L, Lu M, Li C, Xu K, Zhang L (2019): A failed top-down control from the prefrontal cortex to the amygdala in generalized anxiety disorder: Evidence from resting-state fMRI with Granger causality analysis. Neurosci Lett 707:134314.
32. Warren SL, Zhang Y, Duberg K, Mistry P, Cai W, Qin S, *et al.* (2020): Anxiety and stress alter decision-making dynamics and causal amygdala-dorsolateral prefrontal cortex circuits during emotion regulation in children. Biol Psychiatry 88:576–586.
33. Berman MG, Peltier S, Nee DE, Kross E, Deldin PJ, Jonides J (2011): Depression, rumination and the default network. Soc Cogn Affect Neurosci 6:548–555.
34. Hamilton JP, Furman DJ, Chang C, Thomason ME, Dennis E, Gotlib IH (2011): Default-mode and task-positive network activity in major depressive disorder: Implications for adaptive and maladaptive rumination. Biol Psychiatry 70:327–333.
35. Berman MG, Misic B, Buschkuehl M, Kross E, Deldin PJ, Peltier S, *et al.* (2014): Does resting-state connectivity reflect depressive rumination? A tale of two analyses. Neuroimage 103:267–279.
36. Zhou HX, Chen X, Shen YQ, Li L, Chen NX, Zhu ZC, *et al.* (2020): Rumination and the default mode network: Meta-analysis of brain imaging studies and implications for depression. Neuroimage 206:116287.
37. Greicius MD, Flores BH, Menon V, Glover GH, Solvason HB, Kenna H, *et al.* (2007): Resting-state functional connectivity in major depression: Abnormally increased contributions from subgenual cingulate cortex and thalamus. Biol Psychiatry 62:429–437.
38. Sheline YI, Price JL, Yan Z, Mintun MA (2010): Resting-state functional MRI in depression unmasks increased connectivity between networks via the dorsal nexus. Proc Natl Acad Sci U S A 107:11020–11025.
39. Davey CG, Harrison BJ, Yücel M, Allen NB (2012): Regionally specific alterations in functional connectivity of the anterior cingulate cortex in major depressive disorder. Psychol Med 42:2071–2081.
40. Koenigs M, Grafman J (2009): The functional neuroanatomy of depression: Distinct roles for ventromedial and dorsolateral prefrontal cortex. Behav Brain Res 201:239–243.
41. Fox MD, Buckner RL, White MP, Greicius MD, Pascual-Leone A (2012): Efficacy of transcranial magnetic stimulation targets for depression is related to intrinsic functional connectivity with the subgenual cingulate. Biol Psychiatry 72:595–603.
42. Baeken C, Marinazzo D, Wu GR, Van Schuerbeek P, De Mey J, Marchetti I, *et al.* (2014): Accelerated HF-rTMS in treatment-resistant unipolar depression: Insights from subgenual anterior cingulate functional connectivity. World J Biol Psychiatry 15:286–297.
43. Avery JA, Drevets WC, Moseman SE, Bodurka J, Barcalow JC, Simmons WK (2014): Major depressive disorder is associated with abnormal interoceptive activity and functional connectivity in the insula. Biol Psychiatry 76:258–266.
44. Shao R, Lau WKW, Leung MK, Lee TMC (2018): Subgenual anterior cingulate-insula resting-state connectivity as a neural correlate to trait and state stress resilience. Brain Cogn 124:73–81.
45. Chuah YML, Venkatraman V, Dinges DF, Chee MWL (2006): The neural basis of interindividual variability in inhibitory efficiency after sleep deprivation. J Neurosci 26:7156–7162.
46. Koenigs M, Holliday J, Solomon J, Grafman J (2010): Left dorsomedial frontal brain damage is associated with insomnia. J Neurosci 30:16041–16043.
47. Zhang Q, Qin W, He X, Li Q, Chen B, Zhang Y, Yu C (2015): Functional disconnection of the right anterior insula in obstructive sleep apnea. Sleep Med 16:1062–1070.
48. Park B, Palomares JA, Woo MA, Kang DW, Macey PM, Yan-Go FL, *et al.* (2016): Aberrant insular functional network integrity in patients with obstructive sleep apnea. Sleep 39:989–1000.
49. Yu S, Guo B, Shen Z, Wang Z, Kui Y, Hu Y, Feng F (2018): The imbalanced anterior and posterior default mode network in the primary insomnia. J Psychiatr Res 103:97–103.
50. Davis M (1998): Are different parts of the extended amygdala involved in fear versus anxiety? Biol Psychiatry 44:1239–1247.
51. Ryder AG, Yang J, Zhu X, Yao S, Yi J, Heine SJ, Bagby RM (2008): The cultural shaping of depression: Somatic symptoms in China, psychological symptoms in North America? J Abnorm Psychol 117:300–313.
52. Khazaie H, Veronese M, Noori K, Emamian F, Zarei M, Ashkan K, *et al.* (2017): Functional reorganization in obstructive sleep apnoea and insomnia: A systematic review of the resting-state fMRI. Neurosci Biobehav Rev 77:219–231.
53. Andrews PW, Thomson JA Jr (2009): The bright side of being blue: Depression as an adaptation for analyzing complex problems. Psychol Rev 116:620–654.
54. Dunbar RIM (2009): The social brain hypothesis and its implications for social evolution. Ann Hum Biol 36:562–572.
55. Badcock PB, Davey CG, Whittle S, Allen NB, Friston KJ (2017): The depressed brain: An evolutionary systems theory. Trends Cogn Sci 21:182–194.
56. Sheline YI, Barch DM, Price JL, Rundle MM, Vaishnavi SN, Snyder AZ, *et al.* (2009): The default mode network and self-referential processes in depression. Proc Natl Acad Sci U S A 106:1942–1947.
57. Grimm S, Boesiger P, Beck J, Schuepbach D, Bermpohl F, Walter M, *et al.* (2009): Altered negative BOLD responses in the default-mode network during emotion processing in depressed subjects. Neuropsychopharmacology 34:932–943.
58. Xia CH, Ma Z, Ciric R, Gu S, Betzel RF, Kaczkurkin AN, *et al.* (2018): Linked dimensions of psychopathology and connectivity in functional brain networks. Nat Commun 9:3003.
59. Grosenick L, Shi TC, Gunning FM, Dubin MJ, Downar J, Liston C (2019): Functional and optogenetic approaches to discovering stable subtype-specific circuit mechanisms in depression. Biol Psychiatry Cogn Neurosci Neuroimaging 4:554–566.
60. Yamashita A, Sakai Y, Yamada T, Yahata N, Kunimatsu A, Okada N, *et al.* (2020): Generalizable brain network markers of major depressive disorder across multiple imaging sites. PLoS Biol 18:e3000966.
61. Dadi K, Rahim M, Abraham A, Chyzhyk D, Milham M, Thirion B, *et al.* (2019): Benchmarking functional connectome-based predictive models for resting-state fMRI. Neuroimage 192:115–134.
62. Zhi D, King M, Hernandez-Castillo CR, Diedrichsen J (2022): Evaluating brain parcellations using the distance-controlled boundary coefficient. Hum Brain Mapp 43:3706–3720.
63. Kaczkurkin AN, Moore TM, Sotiras A, Xia CH, Shinohara RT, Satterthwaite TD (2020): Approaches to defining common and dissociable neurobiological deficits associated with psychopathology in youth. Biol Psychiatry 88:51–62.
64. Helmer M, Warrington S, Mohammadi-Nejad AR, Ji JL, Howell A, Rosand B, *et al.* (2021): On stability of Canonical Correlation Analysis and Partial Least Squares with application to brain-behavior associations. bioRxiv. https://doi.org/10.1101/2020.08.25.265546.